



Topological Data Analysis (TDA) Techniques Enhance Hand Pose Classification from ECoG Neural Recordings

Simone Azeglio^{1,†}, Arianna Di Bernardo^{1,†,*}, Gabriele Penna², Fabrizio Pittatore², Simone Poetto¹, Johannes Gruenwald³, Christoph Kapeller³, Kyousuke Kamada⁴, and Christoph Guger^{3,5}

¹Master Student, Department of Physics, University of Turin, Italy

²Master Student, Biomedical Engineering, Polytechnic University of Turin, Italy

³g.tec medical engineering GmbH, Schiedlberg, Austria

⁴Neurosurgery, Megumino Hospital, Eniwa, Japan

⁵Guger Technologies OG, Graz, Austria

*E-mail: arianna.dibernard@edu.unito.it

ABSTRACT

Electrocorticogram (ECoG) well characterizes hand movement intentions and gestures. In the present work we aim to investigate the possibility to enhance hand pose classification, in a Rock-Paper-Scissor - and Rest - task, by introducing topological descriptors of time series data. We hypothesized that an innovative approach based on topological data analysis can extract hidden information that are not detectable with standard Brain Computer Interface (BCI) techniques. To investigate this hypothesis, we integrate topological features together with power band features and feed them to several standard classifiers, e.g. Random Forest, Gradient Boosting. Model selection is thus completed after a meticulous phase of bayesian hyperparameter optimization. With our method, we observed robust results in terms of accuracy for a four-labels classification problem, with limited available data. Through feature importance investigation, we conclude that topological descriptors are able to extract useful discriminative information and provide novel insights. Since our data are restricted to single-patient recordings, generalization might be limited. Nevertheless, our method can be extended and applied to a wide range of neurophysiological recordings and it might be an intriguing point of departure for future studies.

I INTRODUCTION

A ECoG

A Brain Computer Interface (BCI) is a device that records the electrical activity of the brain and outputs it directly to the computer in order to be collected and analysed. Nowadays, a wide range of BCI techniques are employed for different purposes,

ranging from medical applications to education and gaming [1]. There are many types of BCI, working on different spatial and temporal resolution. BCI based on electroencephalogram (EEG) are the most widely used. This is due to the low cost and non-invasive set up as well as the high temporal resolution. They are based on the extraction of features from the EEG signal by processing event-related potentials (ERP) or oscillatory activity such as event-related synchronization/desynchronization (ERS/ERD) in the low frequency bands, up to 50 Hz. The most common type of feature based on oscillatory activities is the power band feature, which represents the power of a certain frequency range for each channel [2]. However EEG based BCI have their weakness in the low spatial resolution and low spatial to noise-ratio [3]. Furthermore, the electrical potentials measured in the EEG suffer from a "smearing" phenomenon caused by the different electrical conductivities of the layered structure of the head [4]. Invasive techniques such as electrocorticography (ECoG) or micro-electrode arrays (MEAs) [5] can overcome these issues. In particular ECoG provides a better signal quality [6] and yields a higher spatial resolution than EEG thanks to the small exposure diameter and higher density of the electrodes, as well as its higher invasiveness. Furthermore ECoG signal contains information up to 500 Hz, allowing the study of the powerbands in the high gamma activation (HGA) range, over 40 Hz [3].

B A Multiclass Classification Problem

A key problem in BCI-based neural prosthesis control is decoding movement intentions from brain electrical activity. ECoG signals contain rich information correlated with motor activities, in particular with regards to hand gesture decoding [7]. Such a problem has received a lot of attention recently [8],[9], and can be seen in form of a multiclass classification problem. In this context, each hand gesture corresponds to

[†]These authors contributed equally

a class, and the recorded ECoG signals are the objects to be classified. Previous studies approached this issue as a 3 class classification problem, classifying only the movement trials and ignoring the rest state [8]. In our work we'll deal with 4 classes, considering the rest state as an independent class.

The standard technique used to face such a classification problem is a combination of common spatial patterns (CSP) and multi-class linear discriminant analysis (LDA) [3], or multi-class support vector machine (SVM) [10],[11]. Other studies suggest to use recurrent neural networks to exploit the temporal information in ECoG signals [7].

In this study, we propose a Topological Data Analysis (TDA) based approach, that in combination with standard techniques from the BCI field, aims to provide a robust hand gesture decoding.

II MATERIAL AND METHODS

A Subject

For this study, we evaluated ECoG recordings of one patient (male, 26 years old), who suffered from intractable epilepsy and thus underwent surgical treatment at Asahikawa Medical University, Asahikawa, Japan. In the course of this treatment, a total of 140 ECoG electrodes were implanted on his right hemisphere. From these 140 electrodes, a high-density grid of 60 electrodes (Unique Medical Co., Ltd.; diameter 1.5 mm, spacing 5 mm, geometry 6×10) covered sensorimotor areas. We used these 60 electrodes for further processing.

The patient voluntarily participated in research experiments besides the standard clinical procedure. These research experiments were approved by the institutional review board of Asahikawa Medical University and received certificate number 245 in June 2012. The patient provided written informed consent before participating in the experiments. For additional details (such as detailed electrode placement), we refer to [8], where this patient appears as S2.

B Experimental protocol

We here analyze ECoG data acquired during a hand motor experiment inspired by the famous hand game *rock-paper-scissors*. Specifically, we instructed the patient to form one of the three hand poses (rock, paper, or scissors) according to a visual stimulus presented on a computer screen. These visual stimuli were presented to the patient for one second each and were interleaved by a distorted image shown for a randomized duration between 1.5 and 2.5 seconds. While the distorted image was shown, the patient was asked to return into a relaxed hand position. Consequently, this experiment constitutes a three-class motor control BCI experiment. We analyzed 30 trials per class for this subject in total.

C Data Acquisition

We used a *g.HIamp* biosignal amplifier (g.tec medical engineering GmbH, Austria) to digitize the neural recordings at a sampling rate of 1.2 kHz. For stimulus presentation, we employed the *g.HIsys Highspeed Online Processing* toolbox (g.tec medical engineering GmbH, Austria) in the *Simulink* environment (The MathWorks, Inc., Massachusetts, USA). We saved the raw data as *MATLAB* files on a hard drive for further processing.

D Preprocessing

The first operation performed was the re-referencing of the data by applying a common average reference (CAR) spatial filter, presented in [12]. The CAR filter subtracts, for every time-point and every channel, the mean of all the non-excluded channel, as in [8].

The powerline frequency (50 Hz) was eliminated using a cascade of Notch Butterworth filters of order 5 up to the sixth harmonic, as in [8]. No channels selection strategy were applied. After literature studies [13] we evaluated the signal in different bands. The ECoG signal presents information content up to 500 Hz [14]. For the feature extraction discussed in point F based on the Topological Data Analysis (TDA) method, different frequency bands were evaluated: (i) 1-500 Hz signal in order to evaluate also the low-frequency band (1-50 Hz), removing the DC offset, (ii) 100-500 Hz signal to evaluate only the high-gamma frequency information content, (iii) 50-300 Hz signal to assess a different bandcut which allows the evaluation of the high gamma frequency range band, as done in [8], (iv) 1-500 Hz signal not filtered with the spatial CAR filter.

A further preprocessing step was completed for preparing the signals for the TDA phase, but not for the power band extraction one. When dealing with computational TDA techniques, signals of equal length are required. *Zero-padding* was employed to uniform variable length signals: zero values was appended to the shorter vectors. The padding was applied to the end of the vectors.

E Feature Extraction: Power Band

For the power band features extraction only the CAR filter and the Notch filter were applied. To extract the power band features three different bandwidth were used: 60-90 Hz, 110-140 Hz and 160-190 Hz as in [3]. The bandpass windows were chosen in order to avoid the powerline interference. A 4th order Butterworth filter was used for each temporal filter T_{fb} .

$$y(t) = T_{fb}[x(t)] \quad (1)$$

The filtered signals were then segmented into 2s epochs, each corresponding to a rest/movement trial. To estimate the band power each channel was squared and averaged over a 2s window. The features were then logarithmically scaled [15].

$$f_{pb} = \log \left(\langle |y(t)|_n^{n+fs \cdot 2} \rangle^2 \right) \quad (2)$$

where $\langle \cdot \rangle$ represents the mean value. A total of 180 features were extracted, 1 per each channel for each frequency band used.

F Feature extraction: Topological Data Analysis

Topological Data Analysis (TDA) refers to a collection of methods used to extract geometric features from complex data [16]. By leveraging algebraic topology and computational geometry it is possible to discover structures in data, that are relevant and robust to noise.

A popular method in TDA is *Persistent Homology* (PH), a technique that analyzes the shape of the data to deduce their intrinsic properties, like holes or connected components [17]. PH can be applied to an heterogeneous variety of datasets (images, graphs, time series) by approximating them into elementary objects that preserve their topological properties, and referred to as *simplicial complexes* [18].

In this section we aim to introduce the basic tools utilized in PH. A detailed description of this research area can be found in [19], [20].

Point clouds. In the present work, the intent is to apply PH to preprocessed and segmented ECoG signals. In order to use topological tools on such a multivariate time series, we converted them into point clouds, a suitable data type for PH [21].

To do this we use a modified version of the Takens delay embedding, taking inspiration from [21]. This method consists of sampling the time series at fixed time steps, de facto constructing a point cloud. The Takens embedding is indeed defined on univariate time series, and it depends on three parameters:

- the *time delay* τ is the time between two consecutive values for constructing one embedded point;
- the *dimension* N represents the dimension of the embedding space;
- the *stride* s indicates the duration between two consecutive embedded points.

Here we consider the multivariate time series $\mathbf{X} = \{\mathbf{x}(t_i)\}_{i=1,\dots,T}$, where $\mathbf{x}(t_i) = (x^1(t_i), x^2(t_i), \dots, x^d(t_i)) \in \mathbb{R}^d$, d is the number of 1D time series and T is the length of the series. The stride parameter s determines the sampled times: $s = t_{i+1} - t_i$. By applying the Takens' embedding previously introduced, for a sampled value t_n , we obtain the corresponding point cloud \mathbf{X}_n , defined as follow:

$$\mathbf{X}_n = (\mathbf{x}(t_n), \mathbf{x}(t_n + \tau), \dots, \mathbf{x}(t_n + (N - 1)\tau)) \quad (3)$$

consisting of N points in \mathbb{R}^d .

In the case under consideration, having multivariate time series consisting of 60 channels, we set the dimension parameters to 1. In this way, from every channel, one coordinate value is picked, resulting in a total of 60 coordinates for the embedded points.

The number of points in every point cloud is determined by the stride parameter and by the length of each samples. In the present work we set $s = 10$ and $\tau = 1$. We then obtained a single point cloud for each ECoG signal; where each point cloud is intended as a collection of 240 60-dimensional points.

Simplices and Simplicial Complexes. Once the point clouds were computed for each ECoG sample, we extracted their topological features via PH. The standard technique requires the conversion of the point clouds into *simplicial complexes*, combinatorial structures that preserve the topological properties of the clouds. To be defined, we need the notion of *k-simplex* σ , a convex hull of $k + 1$ affinely independent points $\{v_0, v_1, \dots, v_k\} \in \mathbb{R}^k$:

$$\sigma = [v_0, v_1, \dots, v_k]. \quad (4)$$

A face μ of a *k-simplex* is a simplex of lower dimension, and we write $\mu \subseteq \sigma$. For instance, a 0-simplex is a point, a 1-simplex a segment, a 2-simplex a triangle, and both the 0-simplex and the 1-simplex are faces of the 2-simplex.

A simplicial complex K is then a finite set of simplices such that for every $\mu \subseteq \sigma \in K$, we have $\mu \in K$, and for every $\sigma_1, \sigma_2 \in K$, $\sigma_1 \cap \sigma_2$ is either empty or a face of both.

Finally, we recall the concept of *filtration* of a simplicial complex K , defined as a nested sequence of complexes $\emptyset = K^0 \subseteq K^1 \subseteq \dots \subseteq K^m = K$. Then we refer to K as a *filtered complex*.

When dealing with point cloud data \mathbf{X}_n , the most intuitive type of simplicial complex is the *Vietoris-Rips complex*, i.e. the simplicial complex whose *k*-simplices are determined by each subset of $k + 1$ euclidan point which are pairwise within distance ε :

$$VR_\varepsilon(\mathbf{X}_n) = \{S \subseteq \mathbf{X}_n / d(x(t_n), x(t_m)) \leq 2\varepsilon, \forall x(t_n), x(t_m) \in S\}. \quad (5)$$

In the present work, we computed the Vietoris-Rips complexes for each point cloud previously defined in (3), and then we applied PH.

Homology. Homology is a general technique for associating a sequence of algebraic objects (usually abelian groups) to a topological space K . The so obtained sequence of homology groups $H_k(K)$ provides information about the number of *k*-dimensional "holes" in K for every dimension $k = 0, 1, 2, \dots$

To define the notion of Homology we first introduce the concepts of *chain group* and *boundary operator*.

A *k-chain* is a formal sum of *k*-simplices in *K*:

$$c = \sum_{i=1}^k a_i \sigma_i, \quad a_i \in \{0, 1\}. \quad (6)$$

The set of the *k-chain* in *K* together with the addition operation form the free abelian group $C_k(K)$, referred to as *k-th chain group*.

The boundary operator $\partial_k : C_k(K) \rightarrow C_{k-1}(K)$ is defined on an oriented simplex $\sigma = [v_0, v_1, \dots, v_k]$ by

$$\partial_k(\sigma) = \sum_{i=0}^k (-1)^i [v_0, \dots, \hat{v}_i, \dots, v_k], \quad (7)$$

where the notation \hat{v}_i indicates that the element v_i is excluded from the sum.

In addition we define the *cycle group* $Z_k(K)$ and the *boundary group* $B_k(K)$, both subgroups of $C_k(K)$:

$$\begin{aligned} Z_k(K) &= \ker \partial_k \\ B_k(K) &= \text{Im } \partial_{k+1} \end{aligned} \quad (8)$$

Finally, we obtain the *k-th Homology group* as the quotient group:

$$H_k(K) = Z_k(K) / B_k(K). \quad (9)$$

The *Betti number* β_k is the rank of the *k-th homology group*:

$$\beta_k = \text{rank}(H_k(K)) \quad (10)$$

and indicates the number of *k-dimensional holes* in the simplicial complex *K*. For instance, β_0 counts the number of connected components, β_1 the number of circular holes and β_2 the number of cavities in *K*.

Persistent Homology. The concept of Persistent Homology makes the notion of Homology suitable for computational approaches. The advantage of this technique is the possibility to investigate the homology groups of a topological space at multiple levels of scale.

Given a filtered complex *K*, PH attempts to identify the topological features of *K* that *persist* along the filtration.

For each inclusion $K^i \hookrightarrow K^j$ in the filtration, a homomorphism is naturally induced for each dimension *k*:

$$f_k^{i,j} : H_k(K^i) \rightarrow H_k(K^j) \quad (11)$$

Then, *k-th persistent homology group* is defined as:

$$H_k^{i,j}(K) = \text{Im } f_k^{i,j}, \quad (12)$$

and the *persistent Betti number* is its rank:

$$\beta_k^{i,j} = \text{rank} \left(H_k^{i,j}(K) \right). \quad (13)$$

The *k-th persistent homology* of a filtered simplicial complex gives more refined information than just the homology of the single subcomplexes: structures on data come on multiple scales and can be nested or in more complicated relationships [17].

We can visualize the information given by the *k-th persistent homology group* by drawing the following *Persistence diagram*. The interval $[i, j)$ indicates the lifetime of a *k-homology class* across the filtration: the endpoints of the interval represent the steps of the filtration at which the *k-homology class* born (*i*) or died (*j*), while its difference $l_k^{i,j} = j - i$ represents the *persistence* of the *k-homology class*.

Such an interval can be represented as the point (i, j) in the Euclidean plane \mathbb{R}^2 . All points live in the half-space above the diagonal, and the persistence is easily visible as the vertical distance to the diagonal.

Topological Features. Once the persistence classes of the point clouds \mathbf{X}_n and the persistence diagrams were computed for each homology dimension *k*, we extracted the *topological features*. In the present work, we focused on three classes of features, defined below.

The most intuitive feature we computed was the *Number of Points* in the persistence diagrams, one for each homology dimension that we considered.

We then computed the *Amplitude of a persistence diagram*, defined as its distance to the empty diagram, containing only the diagonal, and it is computed according to the chosen metric (*Wasserstein, Bottleneck, Betti, Landscape, Heat*).

Finally, the *Persistence entropy* measures the entropy of the points in a given persistence diagram. It is computed by taking the Shannon entropy of all persistences in the persistence diagram [22]:

$$E_k = \sum_{[i,j]} \frac{l_k^{i,j}}{L_k} \log \left(\frac{l_k^{i,j}}{L_k} \right) \quad (14)$$

where L_k is the sum of all persistences in the diagram: $L_k = \sum_{[i,j]} l_k^{i,j}$.

In *Table 1* Topological Features are mapped into an integer identifier (ID), which has been used in the implementation and for subsequent figures.

G Machine Learning Pipeline

Once that both Power Band and Topological features have been extracted for each ECoG sample, we decided to stick to

TABLE 1: MAPPING TOPOLOGICAL FEATURES TO INTEGER IDS FOR IMPLEMENTATION

Feature ID	Topological Feature Name	Homology Dimension
0	Bottleneck Amplitude	0
1	Bottleneck Amplitude	1
2	Wasserstein Amplitude	0
3	Wasserstein Amplitude	1
4	Betti Amplitude	0
5	Betti Amplitude	1
6	Landscape Amplitude	0
7	Landscape Amplitude	1
8	Silhouette Amplitude	0
9	Silhouette Amplitude	1
10	Heat Amplitude	0
11	Heat Amplitude	1
12	Normalized Persistence Entropy	0
13	Normalized Persistence Entropy	1
14	Unnormalized Persistence Entropy	0
15	Unnormalized Persistence Entropy	1
16	Number of Points	0
17	Number of Points	1

low-complexity classification models in a supervised machine learning pipeline.

Model selection has been carried out through a careful hyperparameter optimization procedure which is discussed in the next paragraphs. Furthermore, we compared the performances of the algorithms we employed, by training them separately on Power Band features and on Topological features, and we showed that aggregating them considerably improves the performances in both cases.

Model Selection. Specifically, we employed and compared the following classification algorithms: Random Forest, Gradient Boosting, Support Vector Machine, Multilayer Perceptron and Gaussian Naive Bayes. We decided not to utilize any deep learning architecture due to the scarcity of samples: in fact, we had only 180 samples in total, where 90 of them - i.e. 50% - represented the Relax state, 30 the Rock state, 30 the Scissor state and 30 the Paper state.

Given that our problem is multiclass and unbalanced, after hyperparameter optimization, we used 5-fold Stratified Cross Validation and selected the two best models accordingly: Random Forest and Gradient Boosting. Results from the chosen models are shown in *Table 2* and *Table 3*, while all the other tested models are shown in **Appendix**.

Hyperparameters Optimization. Machine learning models usually have several hyperparameters which can be tuned to

TABLE 2: RANDOM FOREST HYPERPARAMETERS OPTIMIZATION AND RESULTS

Features	max_depth	n_estimators	criterion	max_features	Accuracy	Std dev
Power Band	4	100	gini	0.532	0.76	0.06
	7	670	entropy	0.049	0.78	0.03
	8	1497	gini	0.111	0.78	0.05
	9	196	entropy	0.066	0.78	0.04
TDA	8	1500	entropy	1.000	0.80	0.05
	8	1361	entropy	0.131	0.86	0.06
	3	1351	entropy	1.000	0.87	0.05
	4	217	entropy	0.173	0.84	0.05
Power Band + TDA	6	1500	entropy	0.240	0.94	0.04
	6	1037	gini	0.139	0.95	0.03
	5	203	entropy	0.106	0.95	0.04
	5	1500	entropy	0.174	0.96	0.03

change the way the learning process for that algorithm works, e.g. some of them act as regularizers. Modifying their values results in different predictive performance of the algorithm, which are likely tuned for a specific metric, i.e. accuracy in our case. Given that there is not a way to obtain universally optimal hyperparameters for the same algorithm on different data, we would like to find the best way - i.e. the fastest - in order to reach a reasonable accuracy score.

The simplest and most naive automated way is applying vanilla Grid Search: a completely deterministic procedure, where by specifying a range and a granularity for each hyperparameter, the algorithm tries all the possible combinations. Needless to say, the time complexity is exponential in the number of parameters, leading to infeasibility in most of the problems. Another automated method which works reasonably better is Randomized Grid Search, i.e. trying in a random fashion a combination of hyperparameters and selecting the combination which returns the best result. However, there exist an even more efficient way to optimize the hyperparameters: Bayesian optimization [23].

Within the Bayesian optimization framework, we utilize a *surrogate* model to estimate the performance of our predictive algorithm as a function of hyperparameters values. This surrogate model is then used to select the next hyperparameter combination to try. In our specific case, we employed Gaussian Processes as the surrogate model, even though other surrogates might be employed, e.g. Random Forest, Tree-structured Parzen Estimator [24].

Based on this method we selected the two most performing algorithms as classifiers: Random Forest and Gradient Boosting, see *Figure 1* and *Figure 5* in **Appendix** for convergence plots; *Table 2*, *Table 3* and *Table 6*, *Table 7*, *Table 8* in **Appendix** for hyperparameters values as well as accuracy results with respect to the four different preprocessing approaches (1 Hz CAR, 100 Hz CAR, 100 Hz, 50 Hz CAR).

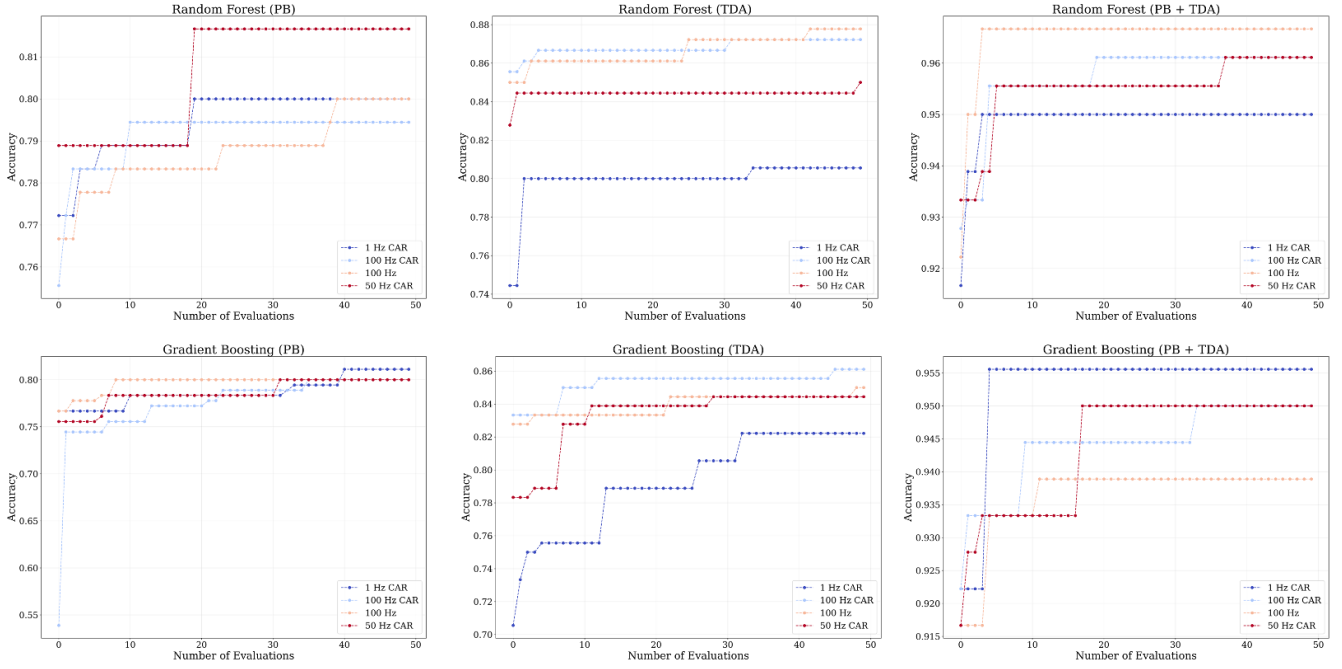


Fig. 1: Convergence plots for Hyperparameter Optimization through Gaussian Processes for Random Forest (Top) and Gradient Boosting (Bottom). From left to right: PB, Power Band Features; TDA, topological data analysis features; PB + TDA, power band and topological aggregated features.

TABLE 3: GRADIENT BOOSTING HYPERPARAMETERS OPTIMIZATION AND RESULTS

Features	max_depth	n_estimators	criterion	subsample	Accuracy	Std Dev
Power Band	3	100	mse	0.474	0.77	0.06
	3	100	mse	0.555	0.77	0.06
	4	554	mse	0.544	0.78	0.06
	3	891	friedman_mse	0.567	0.78	0.05
TDA	6	100	mse	1.000	0.81	0.03
	10	100	mse	0.853	0.85	0.04
	10	1500	friedman_mse	0.880	0.83	0.05
	10	116	friedman_mse	0.934	0.82	0.03
Power Band + TDA	8	446	friedman_mse	0.721	0.94	0.05
	10	886	mse	0.835	0.92	0.06
	4	451	mse	0.399	0.92	0.06
	6	700	mse	0.901	0.93	0.03

Feature Importance. When introducing a novel paradigm for feature extraction, i.e. topological data analysis, it is considered a good practice to quantify whether the information introduced is redundant or not with respect to classical techniques.

A possible model agnostic method is to consider the correlation matrix of features across samples. In **Figure 2**, it is immediate to notice that Topological features (i.e. from 0 to 17) are not at all correlated with Power Band features (i.e. from 18 to 198). Starting from this block diagonal structure, we further investigated the notion of Mutual Information between features and target variables, i.e. labels.

In particular, in **Figure 3** are reported the 10 most infor-

native features, averaged on the four different preprocessing approaches: given that 4-out-of-10, as well as the first one, are Topological features, the impact is inevitably positive. As a comparative analysis, in **Figure 4**, all the 18 Topological features are shown in terms of Mutual Information, see also **Table 1** for TDA features to ID correspondence.

Multicollinearity is evident, due to the block diagonal structure of the correlation matrix. In this case, tackling feature importance with a permutation based approach [25] would not lead to a satisfying result. Since our two best classification models - i.e. Random Forest and Gradient Boosting - are both Tree-Based we opted for a model-specific approach based on node impurity [26]. Node impurity is one of the intrinsic metrics used to split a branch in a Tree-based model, which basically disclose how much of a node belongs to a class. Given that feature importance is a relative measure - i.e. depends on data and specific model - and that we are considering four different preprocessing approaches and two classification models, a sharp way to compare results across different settings would be to consider features' rank. Rank can be further averaged over the different preprocessing approaches and compared from model to model. In **Table 4** and **Table 5** we report feature importance and rank results for each preprocessing approach - e.g *rf_imp* stands for Random Forest feature specific importance on the first preprocessed dataset, *rf_imp_1* on the second preprocessed dataset and so on. As we have foreseen with mutual information,

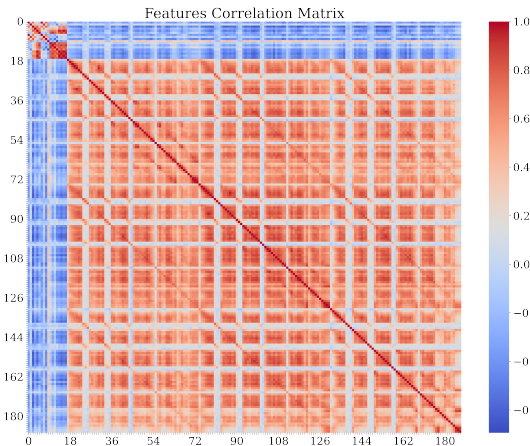


Fig. 2: Features Correlation Matrix. There’s a clear distinction between the first 18 features (from 0 to 17), i.e. topological features, and power band features.

topological features are relevant for both Random Forest and Gradient Boosting classifiers.

The proposed feature importance approach shed light on the relevance of topological features and can be seen an insightful perspective on specific ones, such as feature 16, 14 and 4, respectively *Number of Points* (first dimension), *Persistence Entropy* (first dimension) and *Amplitude with Betti metric* (first dimension).

Different approaches for comparing features’ importance exist: for example, instead of considering the rank, we could have scaled importance measures so that their lowest values are 0 and highest are 1 - i.e. min-max scaling. In the latter case, we might have ended up revealing information about the relative spacing in importance between features and less about their order.

III DISCUSSION

A Discussion of the experimental results

In this section we summarize and comment the experimental results obtained using different classification models.

We start by pointing out the importance and the value of the topological features. Fig. 2 shows the features correlation matrix, and it clearly indicated that TDA and PB features are not correlated. This means that they contain different information that could be useful to use together. The importance of the TDA features is also supported by the feature importance analysis reported in Table 4 and Table 5 and in Fig. 4. In both the models used, topological features appeared among the most informative ones, based on mutual information with the target

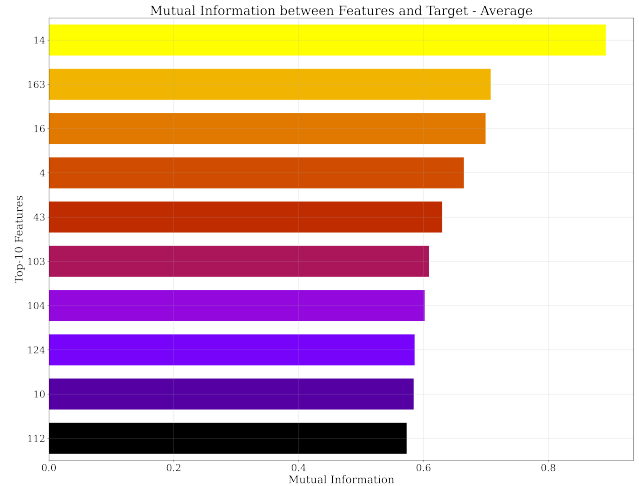


Fig. 3: Mutual Information between Top-10 Features and Target Variables, averaged on the four different preprocessed datasets. Features 14, 16, 4 and 10 are topological.

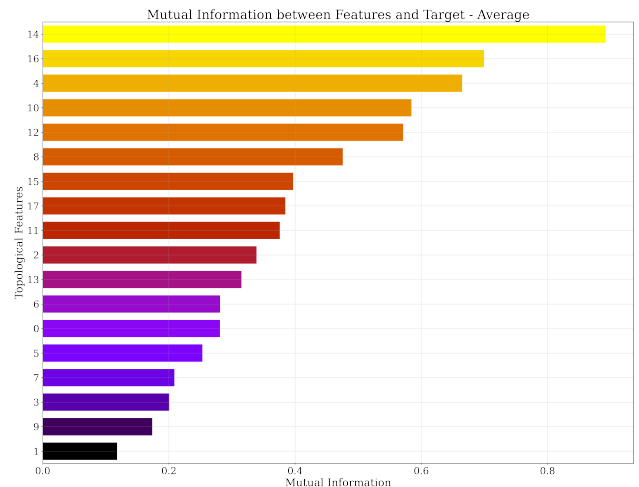


Fig. 4: Mutual Information between Topological Features and Target Variables, averaged on the four different preprocessed datasets

variables. This is remarkable, considering that topological features are outnumbered by power band ones. Finally in Table 2 and Table 3, and in Figure 1, it is possible to see the difference in the performance of the models, by using the two kinds of features alone or aggregated. In both selected models we saw that the usage of PB and TDA features combined leads to the best accuracy. This indicates that the two kind of features represents information that are complementary for the problem of classification.

Established the importance of TDA features we focused on model selection and hyperparameter optimization. Tables 2, 3, 6, 7, 8, indicate that the models with the best performance are Random Forest and Gradient boosting. Among those two, the best results in terms of accuracy are obtained in random forest. With this models it is possible to obtain an accuracy of

TABLE 4: RANDOM FOREST TOP 10 FEATURE IMPORTANCE

Feature ID	rf_imp	rf_rank	rf_imp_1	rf_rank_1	rf_imp_2	rf_rank_2	rf_imp_3	rf_rank_3	avg_imp	avg_rank
16	0.178636	1	0.110822	2	0.117674	1	0.114373	2	0.130376	1.50
14	0.127132	2	0.110936	1	0.113162	2	0.121215	1	0.118111	1.50
4	0.029101	6	0.055215	3	0.056537	3	0.051734	3	0.048147	3.75
103	0.095553	3	0.047188	4	0.046532	4	0.043499	5	0.058193	4.00
163	0.095164	4	0.043100	5	0.043001	5	0.048162	4	0.057357	4.50
43	0.051568	5	0.033094	6	0.030807	8	0.033556	7	0.037256	6.50
112	0.025804	7	0.021518	9	0.014634	13	0.021236	9	0.020798	9.50
10	0.008552	18	0.026356	8	0.033624	7	0.026457	8	0.023747	10.25
122	0.017238	10	0.016938	12	0.017279	11	0.017943	10	0.017350	10.75
123	0.023991	8	0.020730	11	0.016947	12	0.016049	13	0.019429	11.00

TABLE 5: GRADIENT BOOSTING TOP 10 FEATURE IMPORTANCE

Feature ID	gb_imp	gb_rank	gb_imp_1	gb_rank_1	gb_imp_2	gb_rank_2	gb_imp_3	gb_rank_3	avg_imp	avg_rank
16	0.261595	1	0.336517	1	0.178810	2	0.374422	1	0.287836	1.25
122	0.133643	3	0.137376	2	0.058210	3	0.143441	2	0.118168	2.50
103	0.090184	4	0.100476	3	0.049026	4	0.072926	4	0.078153	3.75
14	0.152591	2	0.041389	6	0.204489	1	0.020085	9	0.104638	4.50
154	0.028249	8	0.039477	7	0.032239	7	0.046630	5	0.036649	6.75
4	0.034076	6	0.050935	5	0.017181	13	0.022776	8	0.031242	8.00
10	0.033223	7	0.058431	4	0.009667	21	0.086715	3	0.047009	8.75
124	0.049691	5	0.005141	21	0.021571	11	0.043781	6	0.030046	10.75
43	0.012844	11	0.004685	22	0.048069	5	0.003847	23	0.017361	15.25
47	0.011553	13	0.015106	9	0.002932	41	0.016968	10	0.011640	18.25

0.96, after an accurate hyperparameter optimization. This value of accuracy is obtained from stratified cross validation, and is compatible with the state of the art [8].

B Advantages of this technique

A key component of the proposed method is the usage of TDA as a complementary framework to classical BCI techniques. Such an approach exploits the geometrical properties of the data to infer a particular kind of features with a wide range of advantages.

First of all, features extracted via PH are robust to noise and small perturbation of the input data. Moreover, they are generally invariant for translation, rotation and reflection of the input.

Secondly, they contain information that are different from the ones encoded in the power band features, as shown in **Figure 2**. Such a difference indicates that the topological approach improves our knowledge of the input data and provides additional information to be exploited during the classification phase.

C Limitations

A critical point of our work is the reduced number of ECoG samples we used to carry out the analysis. A single patient recording was in fact considered.

Moreover, we only focused on a specific four-class classification problem. Further analysis should be made to confirm the validity of our method to a wider class of motor experiments and to a different number of classes.

IV FUTURE WORK

The research proposed in this paper is the first, to the best of our knowledge, concrete application of TDA on ECoG neural recordings. Given its prematurity, we would like to further deepen the following aspects:

- In the TDA feature extraction part, we exploited only low-order homology dimensions: higher dimensionality could be considered and compared with the current ones;
- Another interesting perspective is understanding whether it is possible to make our pipeline near-real-time for on-the-field applications, for instance GPU implementations of TDA's techniques - i.e. through *giotto-ph* [27]- or considering Persistent Cohomology based techniques [28]; ;
- Further investigate partial dependence among topological features and power band features, i.e. a reverse-engineering approach might carry some discoveries with respect to the role of specific topological features;
- Try to generalize the same approach on different data: a larger number of patients, different kind of recording (e.g.

EEG) or even other types of time series, in order to attempt to set a standardized pipeline and discern in which cases results are relevant;

- Apply channel exclusion techniques to select the best channels and avoid redundant and noisy information.

V HARDWARE SUPPORT & CODE

We acknowledge the University of Turin's and Polytechnic University of Turin's High Performance Centre for Artificial Intelligence (**HPC4AI**) for providing us with the following computational resources:

- CPU: 12 vCPU Intel Xeon
- RAM: 20 GB RAM ECC
- OS: Ubuntu Server 20.04 LTS
- Python version: 3.7.3
- GPU: Nvidia Tesla T4 (not used yet)

Moreover, the implementation described in the previous paragraphs is largely based on the following libraries: TDA's feature extraction with *giotto-tda* [29], hyperparameter optimization *scikit-optimize* [30] along with Machine Learning algorithms implementation with *scikit-learn* [31].

All the code produced is published on a public repository available at: https://github.com/MachineLearningJournalClub/ECoG_VBH_2021.

VI CONCLUSIONS

The study we carried out had the goal to investigate the applicability of the recently developed field of Topological Data Analysis on time series obtained from neural recordings. We obtained solid evidence that topological features extracted with persistence homology from ECoG data are informative and complementary to standard features as power band. Using both kind of features we observed a significant improvement in classification accuracy of data from a single patient performing hand gestures. More work is needed to validate the efficacy of our approach and to extend it to other cases of study. On the other side, results show potential for attempting to generalize it on different task of classification of neural recordings. The encouraging outcome inspires us to continue our work by testing the methods on more data and possibly devise a standardized TDA pipeline for such a kind of time series.

VII ACKNOWLEDGEMENTS

This work was presented at the *Virtual Brain Hackathon* organized by **g.tec** in April 2021. We acknowledge University of Turin, Polytechnic University of Turin, Machine Learning Journal Club, HPC4AI for supporting us.

REFERENCES

- [1] Jan van Erp, Fabien Lotte, and Michael Tangermann. “Brain-Computer Interfaces: Beyond Medical Applications”. In: *Computer* 45.4 (2012), pp. 26–34.
- [2] F Lotte et al. “A review of classification algorithms for EEG-based brain–computer interfaces: a 10 year update”. In: *Journal of Neural Engineering* 15.3 (Apr. 2018), p. 031005.
- [3] Christoph Kapeller et al. “Single trial detection of hand poses in human ECoG using CSP based feature extraction”. In: *2014 36th Annual International Conference of the IEEE Engineering in Medicine and Biology Society*. IEEE. 2014, pp. 4599–4602.
- [4] R. Hari and A. Puce. *MEG-EEG Primer*. Oxford University Press, 2017. ISBN: 9780190497774.
- [5] Annetta N. et al. Bouton C. Shaikhouni A. “Restoring cortical control of functional movement in a human with quadriplegia”. In: *Nature* 533 (2016), pp. 247–250.
- [6] Yue Li et al. “Gesture decoding using ECoG signals from human sensorimotor cortex: a pilot study”. In: *Behavioural neurology 2017* (2017).
- [7] Gang Pan et al. “Rapid Decoding of Hand Gestures in ElectroCorticography Using Recurrent Neural Networks”. eng. In: *Frontiers in neuroscience* 12 (2018), pp. 555–555. ISSN: 1662-4548.
- [8] Johannes Gruenwald et al. “Time-variant linear discriminant analysis improves hand gesture and finger movement decoding for invasive brain-computer interfaces”. In: *Frontiers in neuroscience* 13 (2019), p. 901.
- [9] Cynthia A Chestek et al. “Hand posture classification using electrocorticography signals in the gamma band over human sensorimotor brain areas”. In: *Journal of Neural Engineering* 10.2 (2013), p. 026002.
- [10] Yue Li et al. “Gesture Decoding Using ECoG Signals from Human Sensorimotor Cortex: A Pilot Study”. eng. In: *Behavioural neurology 2017* (2017), pp. 3435686–12. ISSN: 0953-4180.
- [11] Yanagisawa et al. “Real-time control of a prosthetic hand using human electrocorticography signals”. In: *Journal of Neurosurgery JNS* 114.6 (2011), pp. 1715–1722.
- [12] Laura Leuchs. “Choosing your reference—and why it matters”. In: *Brain Products* (2019), pp. 03–05.
- [13] Tianxiao Jiang et al. “Power modulations of ecog alpha/beta and gamma bands correlate with time-derivative of force during hand grasp”. In: *Frontiers in neuroscience* 14 (2020), p. 100.
- [14] Richard J Staba et al. “Quantitative analysis of high-frequency oscillations (80–500 Hz) recorded in human epileptic hippocampus and entorhinal cortex”. In: *Journal of neurophysiology* 88.4 (2002), pp. 1743–1752.
- [15] Fabien Lotte. “A Tutorial on EEG Signal Processing Techniques for Mental State Recognition in Brain-Computer Interfaces”. In: (Oct. 2014).
- [16] Larry Wasserman. “Topological Data Analysis”. eng. In: *Annual review of statistics and its application* 5.1 (2018), pp. 501–532. ISSN: 2326-8298.
- [17] Herbert Edelsbrunner and John Harer. *Persistent Homology – a Survey*.
- [18] Herbert Edelsbrunner and John Harer. *Computational topology: an introduction*. American Mathematical Soc., 2010.
- [19] S Biasotti et al. “Describing shapes by geometrical-topological properties of real functions”. eng. In: *ACM computing surveys* 40.4 (2008), pp. 1–87. ISSN: 0360-0300.
- [20] Gunnar Carlsson. “Topological pattern recognition for point cloud data”. eng. In: *Acta numerica* 23 (2014), pp. 289–368. ISSN: 0962-4929.
- [21] Chengyuan Wu and Carol Anne Hargreaves. “Topological machine learning for multivariate time series”. eng. In: *Journal of experimental & theoretical artificial intelligence* (2021), pp. 1–16. ISSN: 0952-813X.
- [22] Adélie Garin and Guillaume Tausin. “A topological reading” lesson: Classification of MNIST using TDA”. In: *2019 18th IEEE International Conference On Machine Learning And Applications (ICMLA)*. IEEE. 2019, pp. 1551–1556.
- [23] Jasper Snoek, Hugo Larochelle, and Ryan P. Adams. “Practical Bayesian Optimization of Machine Learning Algorithms”. In: *Proceedings of the 25th International Conference on Neural Information Processing Systems - Volume 2*. NIPS’12. Lake Tahoe, Nevada: Curran Associates Inc., 2012, pp. 2951–2959.
- [24] James Bergstra et al. “Algorithms for Hyper-Parameter Optimization”. In: *Proceedings of the 24th International Conference on Neural Information Processing Systems*. NIPS’11. Granada, Spain: Curran Associates Inc., 2011, pp. 2546–2554. ISBN: 9781618395993.
- [25] Leo Breiman. “Random forests”. In: *Machine learning* 45.1 (2001), pp. 5–32.
- [26] Leo Breiman et al. *Classification and regression trees*. Routledge, 2017.
- [27] Julian Burella Pérez et al. “Giotto-ph: A Python Library for High-Performance Computation of Persistent Homology of Vietoris-Rips Filtrations”. In: *CoRR* abs/2107.05412 (2021). arXiv: 2107 . 05412. URL: <https://arxiv.org/abs/2107.05412>.

- [28] Vin de Silva, Dmitriy Morozov, and Mikael Vejdemo-Johansson. “Dualities in persistent (co)homology”. eng. In: *Inverse problems* 27.12 (2011), pp. 124003–. ISSN: 0266-5611.
- [29] Guillaume Tautin et al. *giotto-tda: A Topological Data Analysis Toolkit for Machine Learning and Data Exploration*. 2020. arXiv: 2004.02551 [cs.LG].
- [30] Tim Head et al. *scikit-optimize/scikit-optimize: v0.5.2*. Version v0.5.2. Mar. 2018. DOI: 10 . 5281 / zenodo . 1207017. URL: <https://doi.org/10.5281/zenodo.1207017>.
- [31] F. Pedregosa et al. “Scikit-learn: Machine Learning in Python”. In: *Journal of Machine Learning Research* 12 (2011), pp. 2825–2830.

APPENDIX

Random Forest and Gradient Boosting are the most accurate models that we employed. On the other hand, during the model selection, we trained several other models that are reported here in **Appendix** for completeness. In particular, we report hyperparameters for: Support Vector Machine in *Table 6*; Multilayer Perceptron in *Table 7*; and Gaussian Naive Bayes in *Table 8*.

Convergence plots for hyperparameter optimization are also shown in *Figure 5*.

TABLE 6: SUPPORT VECTOR MACHINE HYPERPARAMETERS OPTIMIZATION AND RESULTS

Features	C	kernel	Accuracy	Std Dev
Power Band	0.258	linear	0.80	0.03
	0.152	linear	0.80	0.01
	0.228	linear	0.82	0.01
	7.204	rbf	0.79	0.03
TDA	2.263	linear	0.78	0.03
	10.000	linear	0.84	0.06
	8.255	rbf	0.84	0.05
	0.001	linear	0.84	0.06
Power Band + TDA	3.182	linear	0.92	0.05
	7.047	linear	0.93	0.04
	5.709	linear	0.89	0.05
	9.308	linear	0.92	0.03

TABLE 7: MULTILAYER PERCEPTRON HYPERPARAMETERS OPTIMIZATION AND RESULTS

Features	alpha	Accuracy	Std Dev
Power Band	0.054	0.79	0.05
	0.069	0.79	0.04
	0.043	0.79	0.05
	0.002	0.79	0.05
TDA	0.007	0.45	0.14
	0.021	0.47	0.17
	0.008	0.52	0.15
	0.100	0.44	0.16
Power Band + TDA	0.040	0.46	0.13
	0.100	0.59	0.17
	0.077	0.58	0.20
	0.089	0.50	0.18

TABLE 8: GAUSSIAN NAIVE BAYES HYPERPARAMETERS OPTIMIZATION AND RESULTS

Features	var_smoothing	Accuracy	Std Dev
Power Band	0.0	0.7	0.09
	0.0	0.7	0.09
	0.0	0.7	0.09
	0.0	0.7	0.09
TDA	5.055780e-08	0.73	0.07
	7.497147e-09	0.87	0.07
	1.289194e-10	0.83	0.06
	8.680831e-08	0.86	0.02
Power Band + TDA	3.564985e-08	0.89	0.08
	1.000000e-10	0.93	0.05
	1.231941e-10	0.89	0.10
	1.449855e-08	0.90	0.06

Regarding feature importance, in *Table 9* and *Table 10* we show a full report for Topological Data Analysis features with Random Forest and Gradient Boosting.

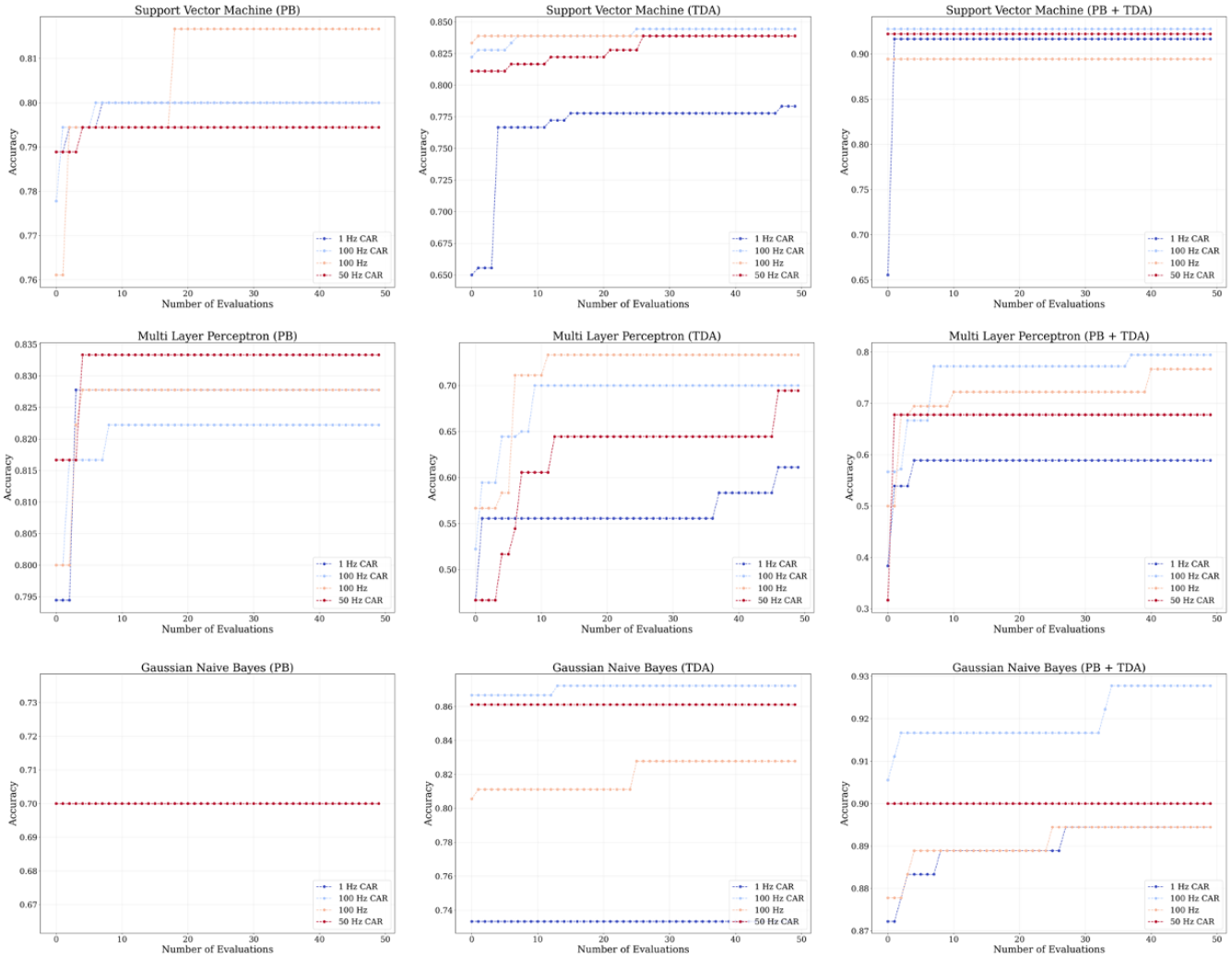


Fig. 5: Convergence plots for Hyperparameter Optimization through Gaussian Processes for Support Vector Machine (Top), Multi-Layer Perceptron (Middle) and Gaussian Naive Bayes (Bottom). From left to right: PB, Power Band Features; TDA, topological data analysis features; PB + TDA, power band and topological aggregated features.

TABLE 9: RANDOM FOREST TDA FEATURE IMPORTANCE

name	rf_imp	rf_rank	rf_imp_1	rf_rank_1	rf_imp_2	rf_rank_2	rf_imp_3	rf_rank_3	avg_imp	avg_rank
14	0.127132	2	0.110936	1	0.113162	2	0.121215	1	0.118111	1.50
16	0.178636	1	0.110822	2	0.117674	1	0.114373	2	0.130376	1.50
4	0.029101	6	0.055215	3	0.056537	3	0.051734	3	0.048147	3.75
10	0.008552	18	0.026356	8	0.033624	7	0.026457	8	0.023747	10.25
12	0.005354	32	0.030151	7	0.033964	6	0.035990	6	0.026365	12.75
17	0.012191	14	0.010846	19	0.010696	21	0.009280	25	0.010753	19.75
15	0.013121	12	0.010451	20	0.008462	24	0.005332	37	0.009342	23.25
2	0.000869	78	0.016206	13	0.017977	10	0.016756	11	0.012952	28.00
8	0.000688	99	0.020956	10	0.018782	9	0.004670	41	0.011274	39.75
11	0.002034	49	0.003632	49	0.003726	49	0.005071	40	0.003616	46.75
5	0.003089	42	0.004433	45	0.002178	66	0.004030	46	0.003432	49.75
3	0.000534	125	0.007971	30	0.003724	50	0.003557	51	0.003946	64.00
6	0.000389	158	0.008211	27	0.009874	22	0.000954	117	0.004857	81.00
7	0.000221	194	0.006495	35	0.005858	35	0.001861	75	0.003609	84.75
13	0.000752	87	0.001901	71	0.001986	70	0.000848	130	0.001372	89.50
0	0.000265	187	0.006695	34	0.007989	25	0.000762	142	0.003928	97.00
1	0.000398	155	0.005212	42	0.000989	115	0.000672	157	0.001817	117.25
9	0.000208	197	0.001170	102	0.000603	166	0.000691	154	0.000668	154.75

TABLE 10: GRADIENT BOOSTING TDA FEATURE IMPORTANCE

name	gb_imp	gb_rank	gb_imp_1	gb_rank_1	gb_imp_2	gb_rank_2	gb_imp_3	gb_rank_3	avg_imp	avg_rank
16	2.615949e-01	1	3.365172e-01	1	1.788097e-01	2	3.744219e-01	1	0.287836	1.25
14	1.525905e-01	2	4.138910e-02	6	2.044894e-01	1	2.008486e-02	9	0.104638	4.50
4	3.407584e-02	6	5.093473e-02	5	1.718133e-02	13	2.277583e-02	8	0.031242	8.00
10	3.322310e-02	7	5.843127e-02	4	9.666783e-03	21	8.671493e-02	3	0.047009	8.75
9	1.811378e-03	38	8.254497e-03	13	9.991055e-04	65	8.593028e-03	15	0.004915	32.75
17	3.225699e-04	78	1.122728e-03	51	2.647563e-02	8	6.483156e-04	48	0.007142	46.25
12	3.263257e-03	29	7.942677e-03	14	1.845400e-05	134	2.624634e-03	28	0.003462	51.25
5	3.134408e-04	79	3.226526e-03	28	8.243095e-04	73	3.620715e-05	79	0.001100	64.75
15	1.838513e-04	85	1.174390e-07	132	2.269648e-02	10	2.304248e-04	63	0.005778	72.50
0	1.888470e-03	34	2.274994e-03	35	9.701916e-07	165	3.487678e-04	56	0.001128	72.50
2	1.882937e-04	84	1.087475e-03	52	2.042865e-03	47	3.227096e-08	137	0.000830	80.00
6	7.316263e-06	123	1.031175e-03	54	1.140362e-06	163	3.371906e-03	25	0.001103	91.25
8	2.664734e-05	111	3.140498e-06	105	1.040844e-03	64	6.738166e-06	102	0.000269	95.50
7	6.130102e-05	98	1.854843e-06	111	5.076095e-04	87	8.198926e-06	99	0.000145	98.75
11	5.479233e-05	100	5.192072e-04	67	1.720756e-04	105	1.443216e-09	145	0.000187	104.25
1	2.913908e-07	141	8.612808e-06	98	1.069186e-03	63	3.986463e-08	136	0.000270	109.50
3	7.092141e-06	124	1.616030e-12	171	1.502068e-06	158	1.280977e-03	37	0.000322	122.50
13	5.774614e-05	99	3.201980e-09	151	5.165003e-06	146	4.522834e-06	105	0.000017	125.25